Magnetic Interactions in New Fluorite-related Rare Earth Oxides

$LnLn'_2RuO_7$ (Ln, Ln' = rare earths)

Yukio Hinatsu and Yoshihiro Doi

Division of Chemistry, Graduate School of Science, Hokkaido University, Sapporo 060-0810, Japan

Abstract

New fluorite-related quaternary rare earth oxides Pr_2YRuO_7 and La_2TbRuO_7 have been prepared. They crystallize in an orthorhombic superstructure of cubic fluorite with space group *Cmcm*.

Through magnetic susceptibility and specific heat measurements, Pr_2YRuO_7 shows an antiferromagnetic transition at 27 K, which is considerably lowered compared with that for Pr_3RuO_7. Analysis of the magnetic specific heat indicates that the magnetic behavior observed at 27 K for Pr_2YRuO_7 is predominantly due to the magnetic interactions between Ru ions, and that the interactions between the Pr^{3+} and Ru^{5+} ions are also important. La_2TbRuO_7 shows magnetic ordering at 9.0 K, which is ascribed to the magnetic ordering between Ru^{5+} ions from the analysis of the magnetic specific heat data.

1. Introduction

Magnetic properties of compounds containing both rare earth and transition metal have attracted a great deal of interest, because they often show anomalous magnetic behavior derived from interactions of unpaired 4f electrons and d electrons.

Since the 4f electrons are highly localized and are shielded by the surrounding 5s and 5p electrons in the outer shell, the magnetic interactions between 4f electrons in the condensed matter are very weak. Therefore, one of the most challenging problems in the modern chemistry of rare earth compounds is to find a compound in which strong magnetic super-exchange interactions between 4f electrons exist, which give rise to a long-range magnetic ordering at relatively high temperatures, and to elucidate their mechanism.

We have paid our attention on the perovskite-type oxides ABO_3. The perovskites have the flexibility of chemical composition. By selecting large alkaline earth elements such as Sr and Ba at the A site atoms, one can accommodate the rare earth (Ln) with smaller transition elements (M) at the 6-coordinate B sites, forming double perovskites A_2LnMO_6. Among them, the magnetic properties of Ba_2PrRuO_6 is worth noting, i.e., one magnetic transition has been observed and its transition temperature for Ba_2PrRuO_6 is astonishingly as high as 117 K, which is ascribed to the strong magnetic interactions between 4f and 4d electrons [1].

Recently, the rare-earth transition metal oxides with composition Ln_3MO_7 have been widely investigated from the viewpoint of their one-dimensional nature. They have a defect-fluorite structure. The relationship to the fluorite structure is as follows. The fluorite unit

cell for oxides has the composition $M^{4+}{}_4O_8$. If the four tetravalent metal ions are replaced by three trivalent ions (Ln) and one pentavalent ion (M), one oxide vacancy is formed per fluorite cell. Due to the significant differences in radii between the Ln^{3+} and M^{5+} ions, cation ordering occurs on the metal sites and the oxide-vacancy orders on the anion sites. The M^{5+} ion is coordinated with six oxygen ions, forming an MO_6 octahedron. These octahedra share corners forming one-dimensional chains which are oriented along the c-axis.

Many studies have been performed, due to this unique crystal structure and possible related magnetic properties for Ln_3MO_7 compounds (M = Mo [2-4], Ru [5-17], Re [18-21], Os [14, 22-24], and Ir [25-28]), especially for the magnetic properties of compounds containing Ru^{5+} ion at the *M*-site because of its largest possible spin (S = 3/2) among the 4d and 5d transition metals. Among many Ln_3MO_7 compounds, we focus our attention on the Pr_3RuO_7 and Tb_3RuO_7. Pr_3RuO_7 has been reported to magnetically order at 55 K [9]. This ordering temperature is the highest compared with those for other Ln_3MO_7 compounds. On the other hand, Tb_3RuO_7 has the smallest Ln^{3+} ions among Ln_3RuO_7 compounds showing an antiferromagnetic transition at low temperatures [29].

In the structure of Ln_3RuO_7 compounds, there are two kinds of oxygen-coordination environment around Ln ions. One-third of the Ln ions are coordinated by eight oxygen ions and the remaining two-third of the Ln ions are seven-coordinated. In order to clarify why Pr_3RuO_7 shows the high magnetic transition temperature, we tried to prepare $Pr_{3-n}Ln_nRuO_7$ compounds (Ln = Y, Lu; n = 1, 2) in which some Pr ions are replaced by the diamagnetic Y or Lu ions. Similarly, $Tb_{3-n}La_nRuO_7$ compounds (n = 1, 2) compounds were prepared. Through

X-ray diffraction measurements, their structures were determined, and magnetic susceptibility and specific heat measurements were performed from 1.8 to 400 K to study their magnetic properties.

2. Experimental

2.1. Sample Preparation

As starting materials, rare earth sesqui-oxide Ln_2O_3 and ruthenium dioxide RuO_2 were used. For Ln = Pr and Tb oxides, Pr_6O_{11} and Tb_4O_7 were used. Among them, La_2O_3 was fired in advance at 900°C for 12 h. They were weighed in an appropriate metal ratio and the mixtures were ground in an agate mortar. The mixtures were pressed into pellets and then heated in air at 1250 ~ 1300 °C for 12 h. After cooling to room temperature, the pellets were crushed, re-pressed into pellets, and reheated in the same conditions. These procedures were repeated three or four times with several intermediate grindings.

2.2. X-ray Diffraction Analysis

Powder X-ray diffraction profiles were measured using a Rigaku Multi-Flex diffractometer with Cu-*Kα* radiation (λ = 1.5406 Å) equipped with a curved graphite monochromator. The data were collected by step-scanning in the angle range of $10° \leq 2\theta \leq 120°$ at a 2θ step-size of 0.02°.

The X-ray diffraction data were analyzed by the Rietveld technique, using the programs RIETAN-FP [30], and the crystal structure was drawn by using the VESTA program [31].

2.3. Magnetic Susceptibility Measurements

The temperature-dependence of the magnetic susceptibility was measured in an applied field of 0.1T over the temperature range of 1.8K ≤ T ≤ 400K, using a SQUID magnetometer (Quantum Design, MPMS5S). The susceptibility measurements were performed under both zero-field-cooled (ZFC) and field-cooled (FC) conditions. The former was measured upon heating the sample to 400 K under the applied magnetic field of 0.1 T after zero-field cooling to 1.8 K. The latter was measured upon cooling the sample from 400 to 1.8 K at 0.1 T.

2.4. Specific Heat Measurements

Specific heat measurements were performed using a relaxation technique by a commercial heat capacity measuring system (Quantum Design, PPMS) in the temperature range of 1.8-400 K. The sintered sample in the form of a pellet was mounted on a thin alumina plate with Apiezon for better thermal contact.

3. Results and Discussion

3.1. Preparation and crystal structure

In this study, we could prepare Pr_2LnRuO_7 (Ln = Y, Lu) and $Tb_{3-n}La_nRuO_7$ (n = 1, 2) compounds. For PrY_2RuO_7 and $PrLu_2RuO_7$, a single-phase compound was not obtained. Figure 1 (a) shows the X-ray diffraction profile of Pr_2YRuO_7. Crystal structures for Ln_3MO_7 have been reported to be well described in the orthorhombic space group *Cmcm* or $C222_1$ [32]. X-ray and neutron diffraction measurements show that Ln_3RuO_7 have also orthorhombic symmetry with space group *Cmcm* for Ln = La ~ Gd. The diffraction patters are similar to that for the fluorite structure and all reflections appeared to be consistent with the C-centered

conditions, $h + k = 2n$, and $h\ 0\ l$ reflections with odd l are absent. We have analyzed the X-ray diffraction profiles with the same space group *Cmcm*. All the reflections observed could be successfully indexed. For the case of $C222_1$ space group, many very weak $h\ 0\ l$ reflections with odd l should be observed. The crystallographic data determined for Pr_2YRuO_7 are listed in Table 1. The results of the Rietveld analysis for the X-ray diffraction profiles of Pr_2YRuO_7 showed that the eight-coordinated 4*a* site are mostly occupied by the Pr atoms. Figure 2 shows the crystal structure of Pr_2YRuO_7. The RuO_6 octahedra share the O(3) ions, forming an infinite one-dimensional zig-zag chain parallel to the [001] direction. The Ln(1) ions are coordinated by eight oxygen ions and the $Ln(1)O_8$ cubes also form a one-dimensional chain through edge-sharing. The RuO_6 and $Ln(1)O_8$ chains lie alternately parallel to the (100) plane, and the Ln(2) ions are seven-coordinated by oxygen ions between the slabs consisting of these chains. The RuO_6 octahedra in the Pr_2YRuO_7 structure are tilted along the [100] direction (see lower figure of Fig. 2). The structure of Pr_2LuRuO_7 is isostructural with that of Pr_2YRuO_7, and the lattice parameters are a = 10.7865(9), b = 7.3638 (6), and c = 7.4807(6) Å.

Figure 1 (b) shows the X-ray diffraction profile of La_2TbRuO_7. Previously, we reported that $LaTb_2RuO_7$ was crystallized in an orthorhombic superstructure of cubic fluorite with space group *Cmcm* [33]. All the reflections observed could be successfully indexed with the same space group. The structural parameters determined for La_2TbRuO_7 are listed in Table 2. The results of the Rietveld analysis for the X-ray diffraction profiles of La_2TbRuO_7 showed that half of the La atoms are almost situated at the eight-coordinated 4*a* site and the rest half of La atoms and Tb atoms are randomly situated at the seven-coordinated 8*g* site.

3.2. Magnetic properties

3.2.1. Pr_2YRuO_7

The temperature dependence of the magnetic susceptibility for Pr_2YRuO_7 is shown in Fig. 3, together with that for Pr_3RuO_7. Pr_2YRuO_7 shows an antiferromagnetic ordering at 27 K. A divergence between the ZFC and FC susceptibilities has been observed below 10 K. Compared with the magnetic transition temperature for Pr_3RuO_7 (55 K), that for Pr_2YRuO_7 is considerably lowered by the diamagnetic Y substitution for Pr. For the case of Pr_3RuO_7, it is discussed that the antiferromagnetic ordering at 55 K is attributable to the magnetic interactions between Ru ions and the magnetic anomaly observed at 36 K is due to the magnetic interactions between Pr ions [13]. We consider that the magnetic behavior observed at 27 K for Pr_2YRuO_7 is predominantly due to the magnetic interactions between Ru ions, and that the interactions between the Pr^{3+} and Ru^{5+} ions are also important in the magnetic interactions of Pr_2YRuO_7, which is elucidated by the specific heat measurements as described in the following.

Figure 4 is the temperature dependence of the reciprocal magnetic susceptibility for Pr_2YRuO_7. The magnetic susceptibilities obey the Curie-Weiss law in the temperature range between 60 and 400 K. The Curie constant (C) and the Weiss constant (θ) for Pr_2YRuO_7 are obtained to be 3.65 emu·K/mol and +20.3 K. The Curie constant expected for Pr_2YRuO_7 is calculated to be $C_{Pr2YRuO7}$ = 5.08 emu·K/mol by substituting the theoretical magnetic moments of the free ion, μ_{Pr3+} = 3.58 μ_B and μ_{Ru5+} = 3.87 μ_B into the equation, $C_{Pr2YRuO7} = 2C_{Pr3+}$ +

C_{Ru5+}. The observed Curie constant is smaller than the calculated one, which suggests that the magnetic ions in this compound may be affected by the crystal field to some extent. The same discussion has been found in the result for Pr_3RuO_7 [9, 13]. For Pr_3MO_7 (M = Nb, Ta, or Sb) compounds containing diamagnetic M ions, the effective magnetic moments of Pr^{3+} have been obtained to be 3.5~3.6 μ_B [34-36], which is close to the theoretical magnetic moment of free Pr^{3+} ion. The positive Weiss constant is obtained for Pr_2YRuO_7, which is the same result for Pr_3RuO_7 (θ = +39.2 K).

In order to obtain the information about the magnetic transition observed at 27 K, specific heat measurements were performed in the temperature range between 1.8 and 400 K. Figure 5 shows the temperature dependence of the specific heat divided by temperature (C_p/T) for Pr_2YRuO_7. A specific heat anomaly has been observed at 27 K, which is in accordance with the results by magnetic susceptibility measurements.

For magnetic compounds, the total specific heat (C_p) is the sum of the lattice specific heat (C_{lat}) and magnetic specific heat (C_{mag}). To evaluate the magnetic contribution to the specific heat, we have to subtract the contribution of lattice specific heat from the total specific heat, i.e., $C_{mag} = C_p - C_{lat}$. The lattice specific heat was estimated by using the specific heat data for a diamagnetic compound La_3NbO_7. The magnetic specific heat below 1.8 K was extrapolated by the relation $C_{mag} \propto T^3$ from the spin-wave model for the antiferromagnet (the dashed line of Fig. 5) [37]. From the temperature dependence of the magnetic specific heat, the magnetic entropy change (S_{mag}) for Pr_2YRuO_7 is calculated by the relation $S_{mag} = \int (C_{mag}/T) dT$. Its temperature dependence is also shown in Fig. 5. The magnetic entropy

change is ~ 12.5 J/(mol K). The maximum magnetic entropy change for the ordering of magnetic moments of Ru^{5+} ions (with a total spin quantum number S = 3/2) is estimated to be R ln(2S+1) = R ln(2·3/2+1) = Rln4 = 11.52 J/(mol K) (R: gas constant). The magnetic entropy change observed from the specific heat measurements is larger than this value, indicating that the magnetic moments of Pr^{3+} ions also contribute to the magnetic interactions between Ru^{5+} ions observed at 27 K. The magnetic interaction in Pr_2YRuO_7 compound is via the pathway of Pr-O-Ru. This result suggests that the remarkable decrease of magnetic transition temperature for Pr_2YRuO_7 compared with that for Pr_3RuO_7 is due to the magnetic dilution of Pr sub-lattice by the diamagnetic Y^{3+} ions.

The magnetic properties of Pr_2LuRuO_7 are quite similar to those of Pr_2YRuO_7, and the magnetic transition temperature is 27 K, which is the same temperature as that for Pr_2YRuO_7.

3.2.2. $Tb_{3-n}La_nRuO_7$ (n = 1, 2)

Figure 6 depicts the temperature dependence of the magnetic susceptibility for Tb_3RuO_7, $LaTb_2RuO_7$, and La_2TbRuO_7. Previous studies on Tb_3RuO_7 and $LaTb_2RuO_7$ show that there exist two magnetic transitions and their transition temperatures (10 and 17 K) are the same between these two compounds [29, 33]. Measurements and analysis of their specific heat and magnetic susceptibility data on Tb_3RuO_7 and $LaTb_2RuO_7$ indicate that the magnetic transitions at 10 and 17 K are due to the magnetic ordering of Tb^{3+} and Ru^{5+} ions, respectively. Different from the case of Tb_3RuO_7 and $LaTb_2RuO_7$, one magnetic anomaly has been found at 9.0 K for La_2TbRuO_7. A divergence between the ZFC and FC susceptibilities has been

observed below this temperature. We consider that this magnetic anomaly is due to the magnetic interactions between Ru^{5+} ions, which will be elucidated in later.

Figure 7 shows the reciprocal magnetic susceptibility vs. temperature curve for La_2TbRuO_7. In the paramagnetic temperature region, the Curie-Weiss law fitting was applied to the temperature dependence of the susceptibility. The effective magnetic moment and the Weiss constant for La_2TbRuO_7 were obtained to be 10.1 μ_B and -9.2 K, respectively. Since both Tb^{3+} and Ru^{5+} ions contribute to the paramagnetic behavior of La_2TbRuO_7, its effective magnetic moment should be calculated from the equation $\mu_{calc} = \sqrt{\mu_{Tb^{3+}}^2 + \mu_{Ru^{5+}}^2}$. The theoretical effective magnetic moment of Tb^{3+} is 9.72 μ_B, and the effective magnetic moment of Ru^{5+} experimentally obtained for Tb_3RuO_7 is 3.58 μ_B [29]. Using these values, the effective magnetic moment of La_2TbRuO_7 is calculated to be 10.36 μ_B. The moment experimentally obtained for La_2TbRuO_7 is near to this value. The negative Weiss constant indicates that the magnetic transition observed at 9.0 K is antiferromagnetic.

In order to obtain the information about the low-temperature magnetic behavior of La_2TbRuO_7, specific heat measurements were performed down to 1.8 K. Figure 8 shows the temperature dependence of the specific heat divided by temperature (C_p/T) for La_2TbRuO_7. The specific heat data for Tb_3RuO_7 and $LaTb_2RuO_7$ are also shown in the same figure. Different from the case of Tb_3RuO_7 and $LaTb_2RuO_7$, one specific heat anomaly has been observed around 9.0 K, which is in accordance with the results by magnetic susceptibility measurements.

The magnetic specific heat was estimated by subtracting the contribution of the lattice

specific heat from the total specific heat in the same way as is the case for Pr_2YRuO_7. The lattice specific heat was estimated by using the data for a diamagnetic compound La_3NbO_7. Figure 9 shows the temperature dependence of the magnetic specific heat divided by temperature (C_{mag}/T). From the temperature dependence of the magnetic specific heat, the magnetic entropy change for La_2TbRuO_7 (S_{mag}) is calculated by the relation $S_{mag} = \int (C_{mag}/T) dT$, and its temperature dependence is also shown in Fig. 9. The total magnetic entropy change amounts to ~ 11 J/mol K at 40 K. The maximum magnetic entropy change for the ordering of magnetic moments of Ru^{5+} ions is estimated to be 11.52 J/(mol K). The estimated S_{mag} value from specific heat measurements is in agreement with this value. Compared with the Tb_3RuO_7, two-thirds of the Tb sites are occupied by diamagnetic La^{3+} ions in the La_2TbRuO_7 compound. Therefore, the Tb^{3+} ions no longer contribute to the magnetic ordering of Ru^{5+} ions in the La_2TbRuO_7 compound, that is, the magnetic anomaly observed at 9.0 K is due to the magnetic ordering of Ru^{5+} ions.

Summary

Quaternary rare earth oxides Pr_2YRuO_7 and La_2TbRuO_7 crystallize in an orthorhombic superstructure of cubic fluorite with space group *Cmcm*.

Magnetic susceptibility and specific heat measurements show that Pr_2YRuO_7 shows an antiferromagnetic transition at 27 K, which is considerably lowered compared with that for Pr_3RuO_7. Analysis of the magnetic specific heat indicates that the magnetic behavior observed at 27 K is predominantly due to the magnetic interactions between Ru ions, and that the

interactions between the Pr^{3+} and Ru^{5+} ions also contribute to them. La_2TbRuO_7 shows magnetic ordering at 9.0 K, which is ascribed to the magnetic ordering between Ru^{5+} ions.

References

[1] Y. Izumiyama, Y. Doi, M. Wakeshima, Y. Hinatsu, Y. Shimojo, and Y. Ishii, *J. Phys.: Condens. Matter*, **13**, 1303-1313 (2001).

[2] J. E. Greedan, N. P. Raju, A. Wegner, P. Gougeon, and J. Padiou, *J. Solid State Chem*., **129**, 320-327 (1997).

[3] H. Nishimine, M. Wakeshima, and Y. Hinatsu, *J. Solid State Chem.*, **178**, 1221-1229 (2005).

[4] M. Wakeshima and Y. Hinatsu, *J. Solid State Chem.*, **183**, 2681-2688 (2010).

[5] F. P. F. van Berkel and D. J. W. IJdo, *Mater. Res. Bull*., **21**, 1103-1106 (1986).

[6] W. A. Groen, F. P. F. van Berkel, and D. J. W. IJdo, *Acta Crystallogr*. Sec. **C 43**, 2262-2264 (1986).

[7] A. Kahn-Harari, L. Mazerrolles, D. Michel, and F. Robert, *J. Solid State Chem*., **116**, 103-106 (1995).

[8] P. Khalifah, R. W. Erwin , J. W. Lynn, Q. Huang, B. Batlogg, and R. J. Cava, *Phys. Rev.*, **B 60**, 9573-9578 (1999).

[9] F. Wiss, N. P. Raju, A. S. Wills, and J. E. Greedan, *Inter. J. Inorg. Mater.*, **2**, 53-59 (2000).

[10] B.P.Bontchev, A.J.Jacobson, M.M.Gospodinov, V. Skumryev, V. N. Popov, B. Lorenz, R. L. Meng, A. P. Litvinchuk, and M.N. Iliev, *Phys. Rev*. **B. 62**, 12235-12240 (2000).

[11] D. Harada and Y. Hinatsu, *J. Solid State Chem.*, **158**, 245-253 (2001).

[12] D. Harada, Y. Hinatsu, and Y. Ishii, *J. Phys.: Condens. Matter*, **13**, 10825-10836 (2001).

[13] D. Harada and Y. Hinatsu, *J. Solid State Chem*., **164**, 163-168 (2002).

[14] R. Lam, F. Wiss, and J. E. Greedan, *J. Solid State Chem.* **167**, 182-187 (2002).

[15] W. R. Gemmill, M. D. Smith, and H-C, zur Loye, *Inorg. Chem*., **43**, 4254-4261 (2004).

[16] N. Ishizawa, K. Hiraga, D. du Boulay, H. Hibino, T. Ida, and S. Oishi, *Acta Cryst*., **E62**, i13-i16 (2006).

[17] Y. Hinatsu and Y. Doi, *J. Solid State Chem.*, **220**, 22-27 (2014).

[18] G. Wltschek, H. Paulus, I. Svoboda, H. Ehrenberg, and H. Fuess, *J.Solid State Chem*. **125**, 1-4 (1996).

[19] R. Lam, T. Langet, and J. E. Greedan, *J. Solid State Chem*. **171**, 317-323 (2002).

[20] Y. Hinatsu, M. Wakeshima, N. Kawabuchi, and N. Taira, *J. Alloys Compd*., **374**, 79-83 (2004).

[21] M. Wakeshima and Y. Hinatsu, *J. Solid State Chem*., **179**, 3575-3581 (2006).

[22] J. R. Plaisier, R. J. Drost, and D. J. W. IJdo, *J. Solid State Chem.* **169**, 189-198 (2002).

[23] W. R. Gemmill, M. D. Smith, Y. A. Mozharivsky, G. J. Miller, and H-C, zur Loye, *Inorg. Chem.*, **44**, 7047-7055 (2005).

[24] Y. Hinatsu and Y. Doi, *J. Solid State Chem.*, **198**, 176-185 (2013).

[25] J. F. Vente and D. J. W. IJdo, *Mater. Res. Bull.*, **26**, 1255-1262 (1991).

[26] H. Nishimine, M. Wakeshima, and Y. Hinatsu, *J. Solid State Chem*., **177**, 739-744 (2004).

[27] Y. Hinatsu, Y. Doi, H. Nishimine, M. Wakeshima, and M. Sato, *J. Alloys Compd*., **488**, 541-545 (2009).

[28] T. Fennell, S. T. Bramwell, and M. A. Green, *Can. J. Phys.*, **79**, 1415-1419 (2001).

[29] Y. Hinatsu and Y. Doi, *J. Solid State Chem.*, **220**, 22-27 (2014).

[30] F. Izumi and K. Momma, *Solid State Phenom.*, **130**, 15-20 (2007).

[31] K. Momma and F. Izumi, *Appl. Crystallogr*., **41**, 653-658 (2008).

[32] H. J. Rossell, *J. Solid State Chem*. **27**, 115-122 (1979).

[33] Y. Hinatsu and Y. Doi, *J. Solid State Chem.*, **233**, 37-43 (2016).

[34] M. Wakeshima, H. Nishimine, and Y. Hinatsu, *J. Phys.: Condens. Matter*, **16**, 4103-4120 (2004).

[35] Y. Doi and Y. Hinatsu, *J. Solid State Chem.*, **182**, 709-715 (2009).

[36] Y. Hinatsu, H. Ebisawa, and Y. Doi, *J. Solid State Chem.*, **182**, 1694-1699 (2009).

[37] S. J. Joshua and A. P. Cracknell, *Phys. Letter*, **A28**, 562-563 (1969).

Figure captions

Fig. 1 Powder x-ray diffraction profiles for (a) Pr_2YRuO_7 and (b) La_2TbRuO_7. The calculated and observed profiles are shown on the top solid line and cross markers, respectively. The vertical marks in the middle show positions calculated for Bragg reflections. The lower trace is a plot of the difference between calculated and observed intensities.

Fig. 2. Schematic crystal structure of $Ln(1)Ln(2)_2RuO_7$. The lower figure is the structure viewed from the [100] direction.

Fig. 3. Temperature dependence of magnetic susceptibility for Pr_3RuO_7 and Pr_2YRuO_7 in the temperature range between 1.8 and 200 K. Blue and red circles are ZFC and FC susceptibility data, respectively.

Fig. 4. Temperature dependence of the reciprocal magnetic susceptibility for Pr_2YRuO_7 in the temperature range between 1.8 and 350 K.

Fig. 5 Temperature dependence of the specific heat divided by temperature (C_p/T) and the magnetic entropy (S_{mag}) for Pr_2YRuO_7 in the temperature range between 1.8 and 150 K.

Fig. 6. Temperature dependence of magnetic susceptibility for (a) Tb_3RuO_7, (b) $LaTb_2RuO_7$, and (c) La_2TbRuO_7 in the temperature range between 1.8 and 100 K. Blue and red circles are ZFC and FC susceptibility data, respectively.

Fig. 7. Temperature dependence of the reciprocal magnetic susceptibility for La_2TbRuO_7 in the temperature range between 1.8 and 350 K.

Fig. 8 Temperature dependence of the specific heat divided by temperature (C_p/T) for

Tb_3RuO_7, $LaTb_2RuO_7$, and La_2TbRuO_7 in the temperature range between 1.8 and 50 K.

Fig. 9. Temperature dependence of the magnetic specific heat divided by temperature (C_{mag}/T) and the magnetic entropy (S_{mag}) for La_2TbRuO_7 in the temperature range between 1.8 and 70 K.

Please change Table 1 into new version as shown below!

- The font size of Pr(1), Y(1), Pr(2), and Y(2) should be the same as that of Ln(1) and Ln(2).
- Pr(1), Y(1), Pr(2), and Y(2) should be roman (not italic).
- Equations in Note of the proof are too large in the font size.

Table 1 Structural parameters for Pr_2YRuO_7.

Atom		Site	occupancy	*x*	*y*	*z*	*B* / Å^2
Ln(1)	Pr(1)/Y(1)	4*a*	0.77(1)/0.23	0	0	0	0.48(6)
Ln(2)	Pr(2)/Y(2)	8*g*	0.61/0.39	0.223(1)	0.306(1)	1/4	0.48
Ru		4*b*	1.0	0	1/2	0	0.30(6)
O(1)		16*h*	1.0	0.132(2)	0.315 (2)	0.954(2)	1.2(2)
O(2)		8*g*	1.0	0.137(3)	0.017(2)	1/4	1.2
O(3)		4*c*	1.0	0	0.419(3)	1/4	1.2

Note. Space group *Cmcm*; a = 10.81923(90) Å, b = 7.36871(62) Å, c = 7.48616(64) Å, V = 596.825(87) Å^3, R_{wp} = 18.86 %, R_B = 2.39 %, and R_e = 10.85 %, where

$$R_{wp} = \left[\sum_i w_i \left(y_i - f_i(\boldsymbol{x}) \right)^2 / \sum_i w_i y_i^{\,2} \right]^{1/2}, \quad R_B = \sum_K \left| I_O(\boldsymbol{h}_K) - I(\boldsymbol{h}_K) \right| / \sum_K I_O(\boldsymbol{h}_K), \text{ and}$$

$$R_e = \left[(N - P) / \sum_i w_i y_i^{\,2} \right]^{1/2}.$$

Please change Table 2 into new version as shown below!

- The font size of La(1), Tb(1), La(2), and Tb(2) should be the same as that of Ln(1) and Ln(2).
- Equations in Note of the proof are too large in the font size.

Table 2 Structural parameters for La_2TbRuO_7.

Atom		Site	occupancy	*x*	*y*	*z*	*B* / Å^2
Ln(1)	La(1)/Tb(1)	4*a*	1.0/0.0	0	0	0	0.72(8)
Ln(2)	La(2)/Tb(2)	8*g*	0.5/0.5	0.221(1)	0.309(1)	1/4	0.72
Ru		4*b*	1.0	0	1/2	0	0.30(6)
O(1)		16*h*	1.0	0.124(2)	0.325(2)	0.960(1)	1.2(2)
O(2)		8*g*	1.0	0.134(2)	0.027(2)	1/4	1.2
O(3)		4*c*	1.0	0	0.436(3)	1/4	1.2

Note. Space group *Cmcm*; a = 11.00604(90) Å, b = 7.43619(71) Å, c = 7.55779(72) Å, V = 618.541(103) Å^3, R_{wp} = 13.94 %, R_B = 2.13 %, and R_e = 10.92 %, where

$$R_{wp} = \left[\sum_i w_i \left(y_i - f_i(\boldsymbol{x}) \right)^2 / \sum_i w_i y_i^{\,2} \right]^{1/2}, \quad R_B = \sum_K \left| I_O(\boldsymbol{h}_K) - I(\boldsymbol{h}_K) \right| / \sum_K I_O(\boldsymbol{h}_K), \text{ and}$$

$$R_e = \left[(N - P) / \sum_i w_i y_i^{\,2} \right]^{1/2}.$$

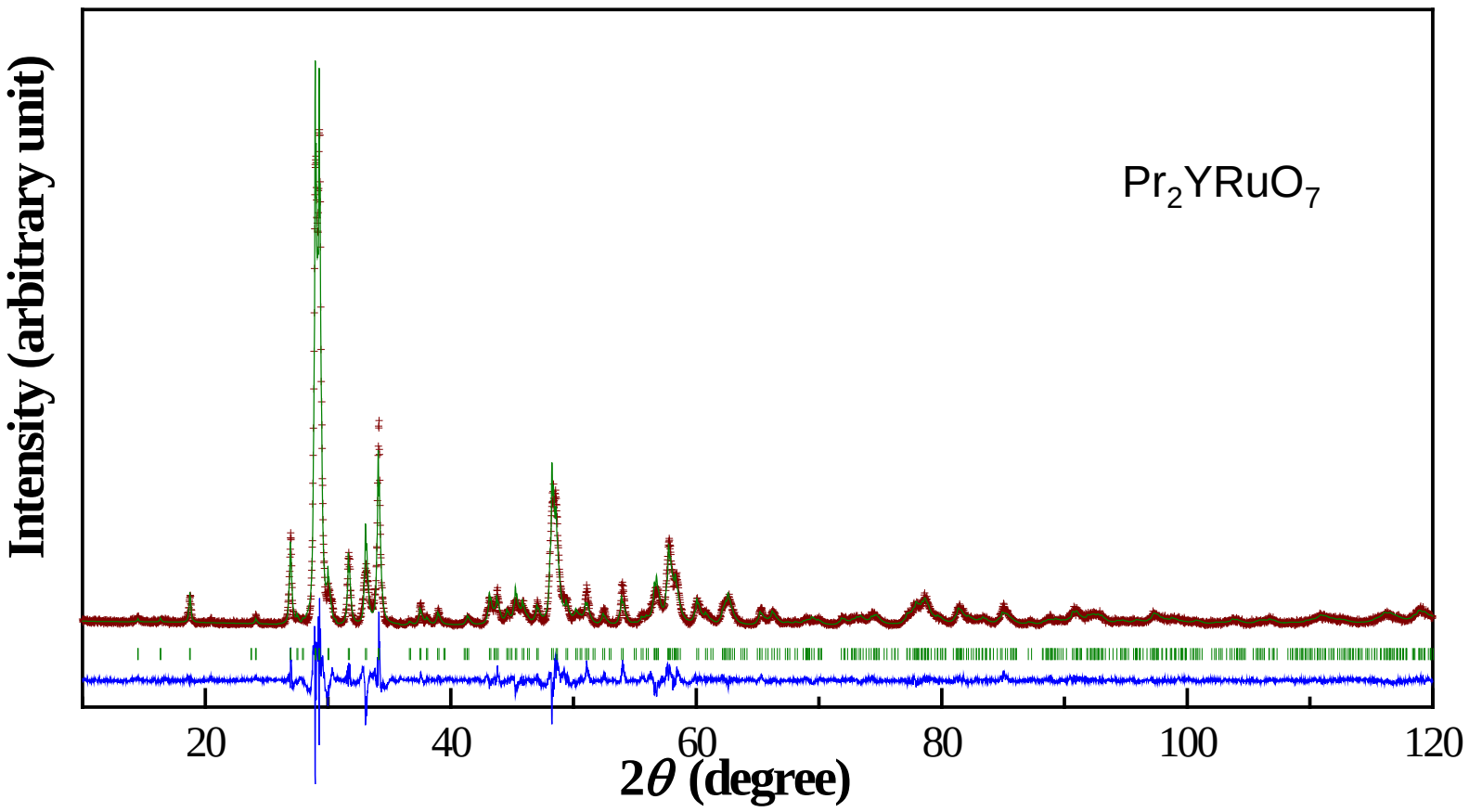
Intensity (arbitrary unit)
Pr2YRuO7
20
40
60
80
100
120
2θ (degree)

Fig. 1 (a)

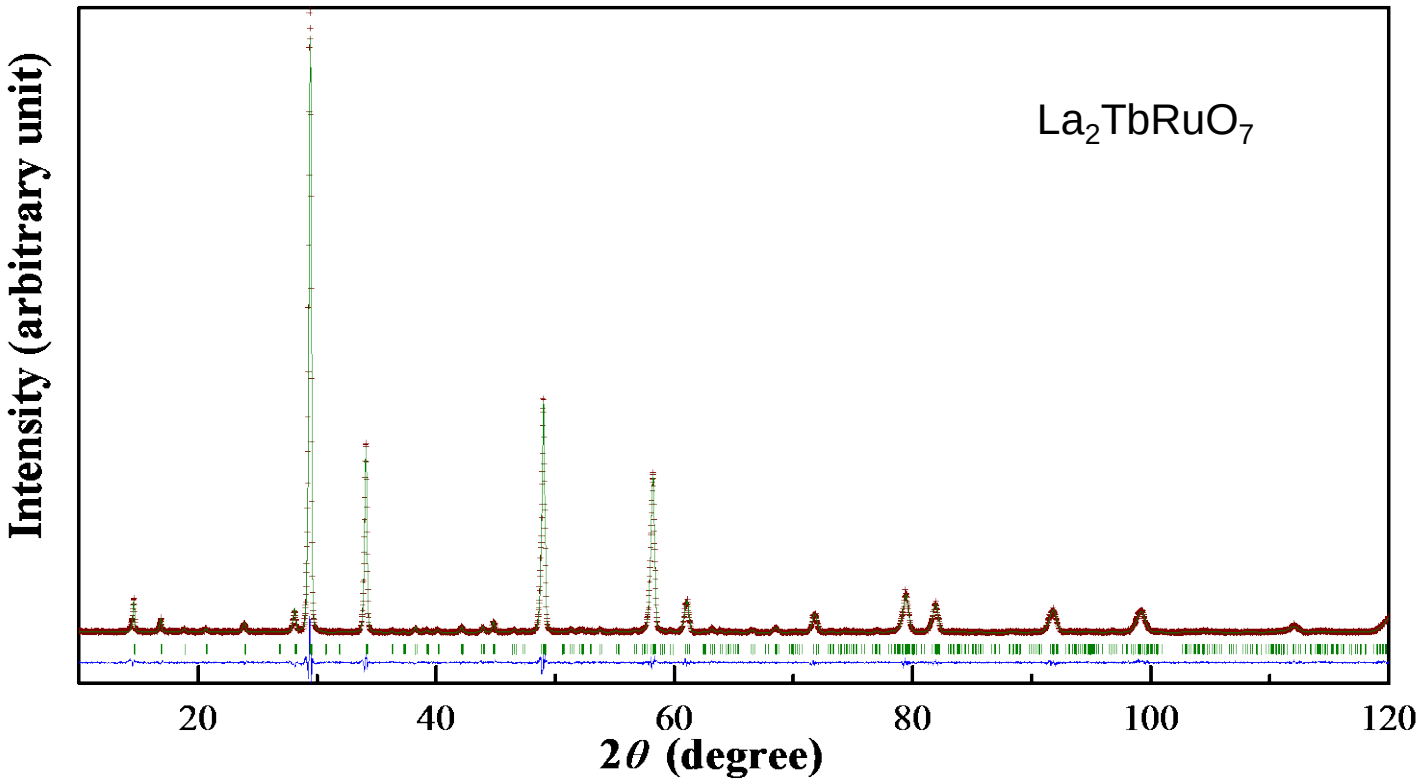
Intensity (arbitrary unit)
La2TbRuO7
20
40
60
80
100
120
2θ (degree)

Fig. 1 (b)

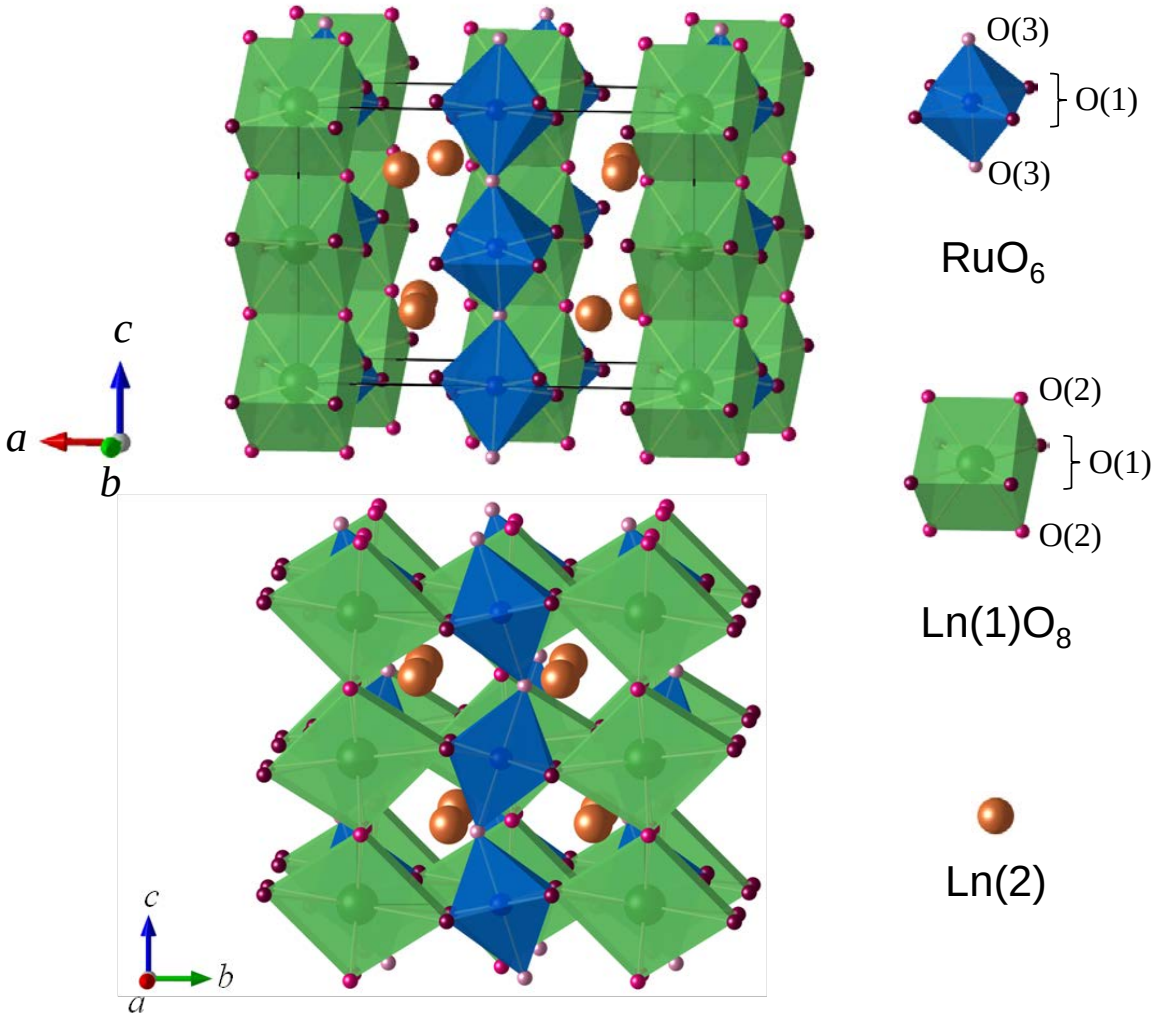

Fig. 2

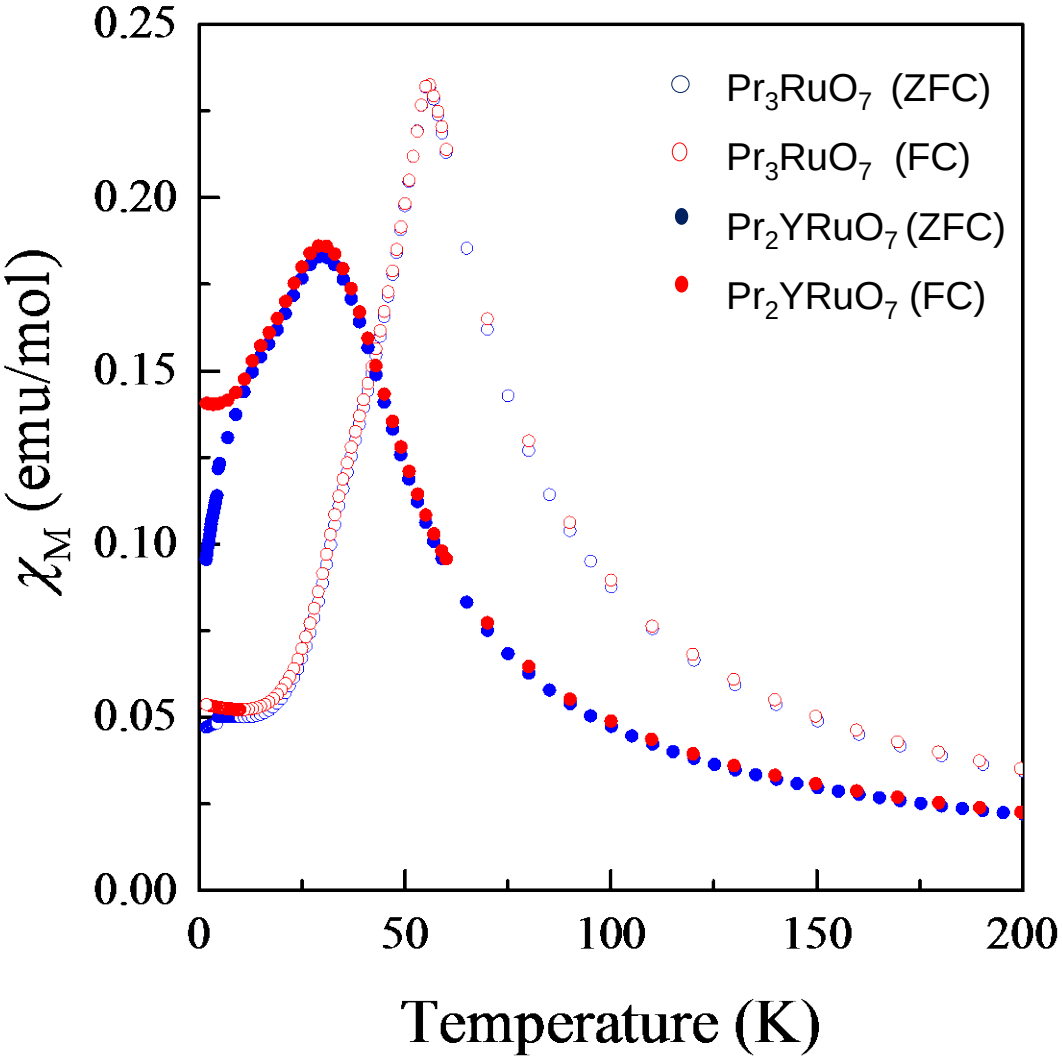
0.25
0.20
0.15
0.10
0.05
0.00
χ_M (emu/mol)
0
50
100
150
200
Temperature (K)
Pr_3RuO_7 (ZFC)
Pr_3RuO_7 (FC)
Pr_2YRuO_7 (ZFC)
Pr_2YRuO_7 (FC)

Fig. 3

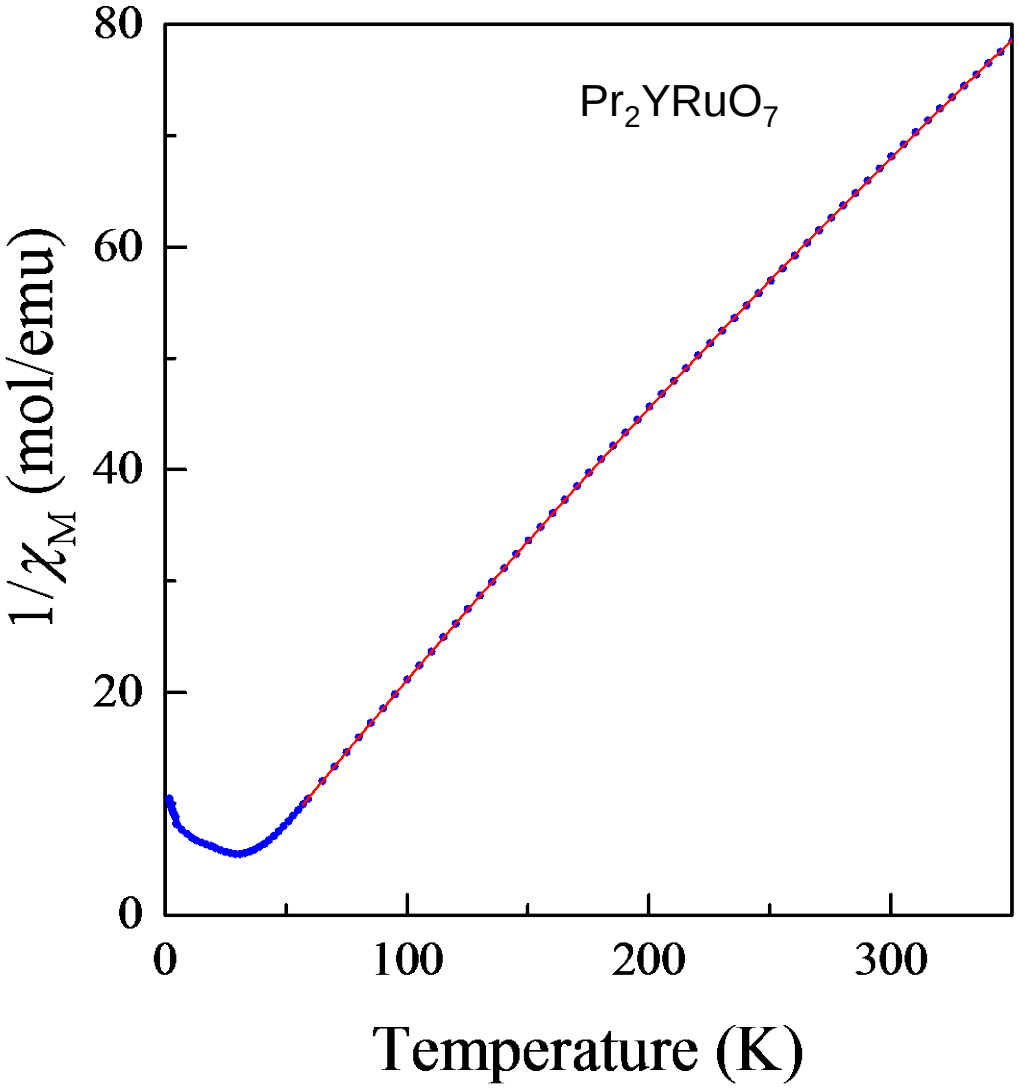

Fig.4

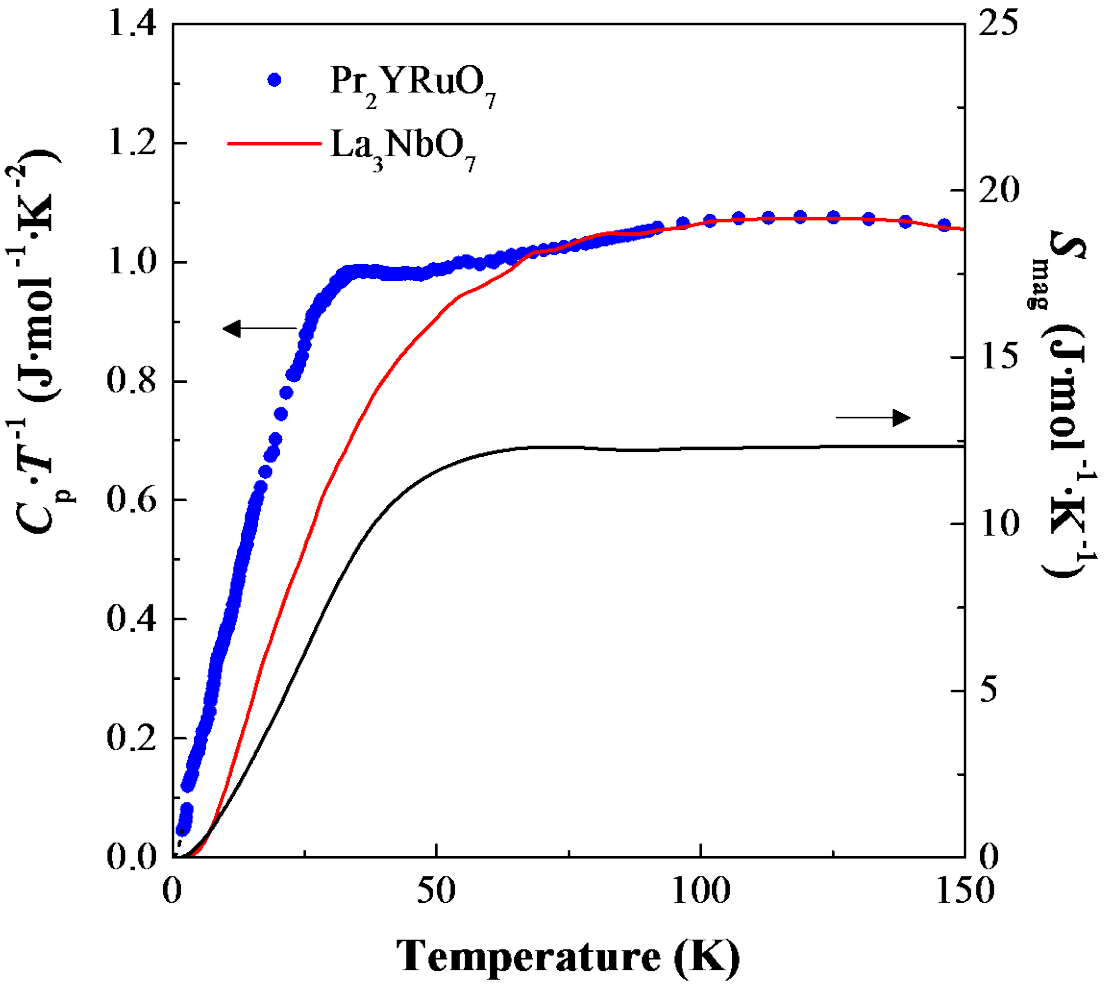
Pr2YRuO7
La3NbO7
Cp·T-1 (J·mol-1·K-2)
Smag (J·mol-1·K-1)
Temperature (K)
0.0
0.2
0.4
0.6
0.8
1.0
1.2
1.4
0
5
10
15
20
25
0
50
100
150

Fig.5

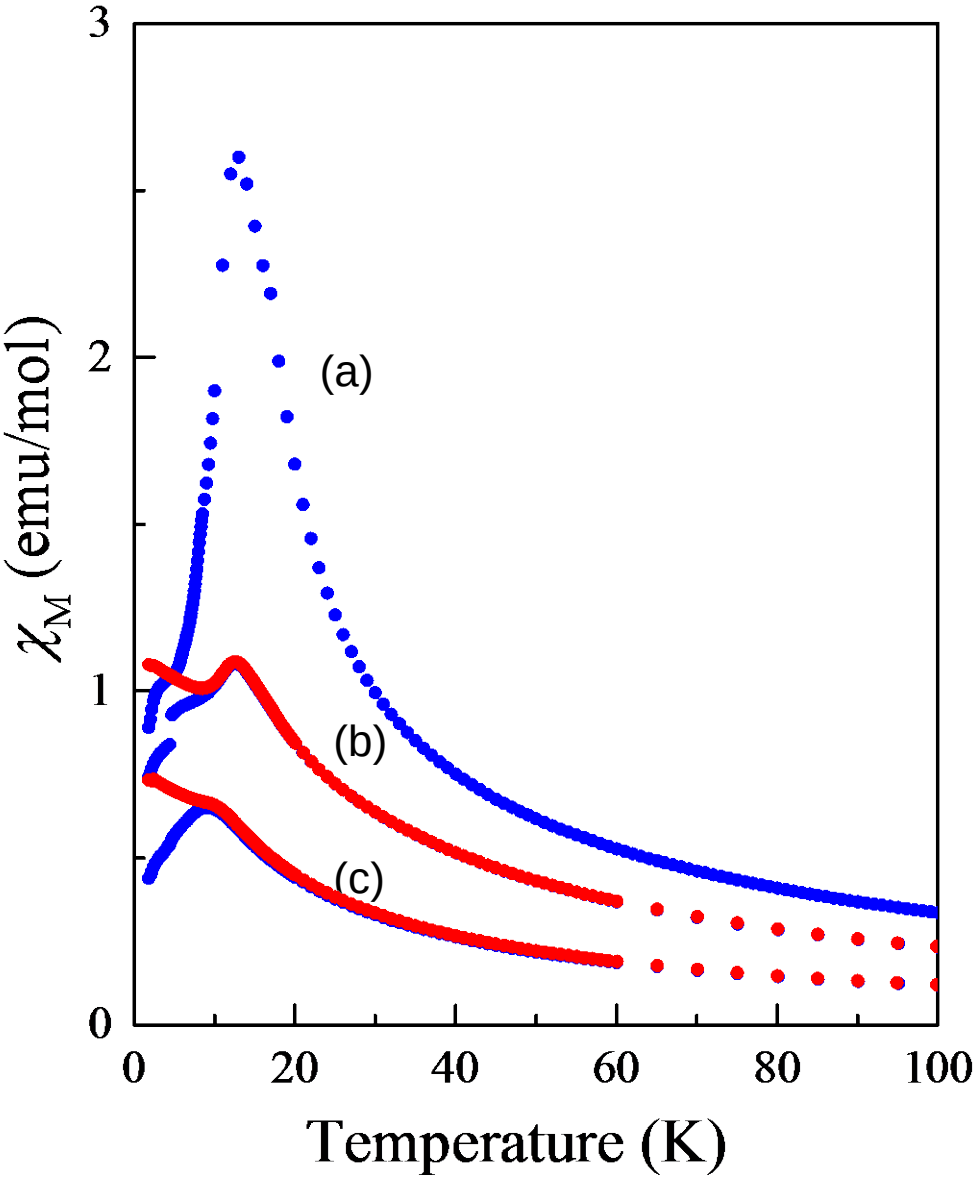

Fig.6

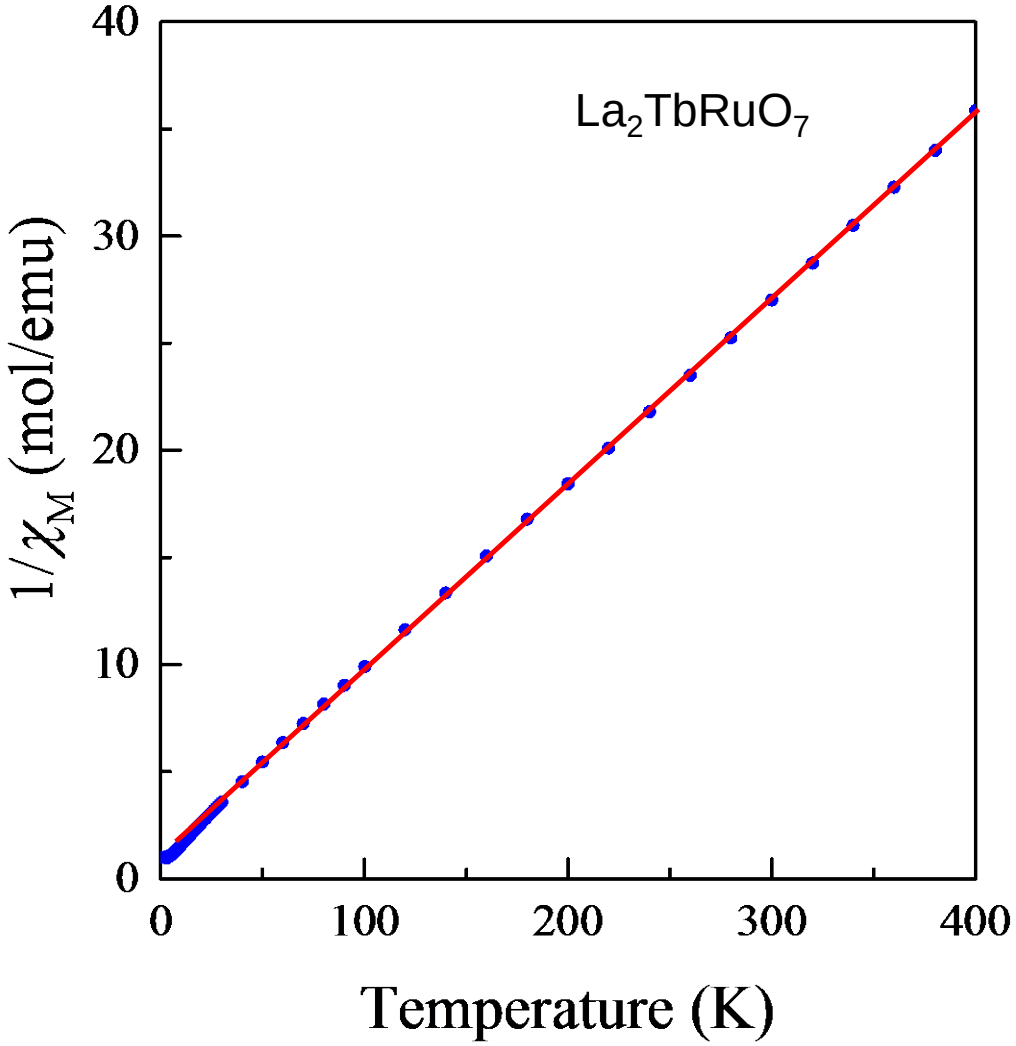
La2TbRuO7
1/χM (mol/emu)
Temperature (K)
0
10
20
30
40
0
100
200
300
400

Fig. 7

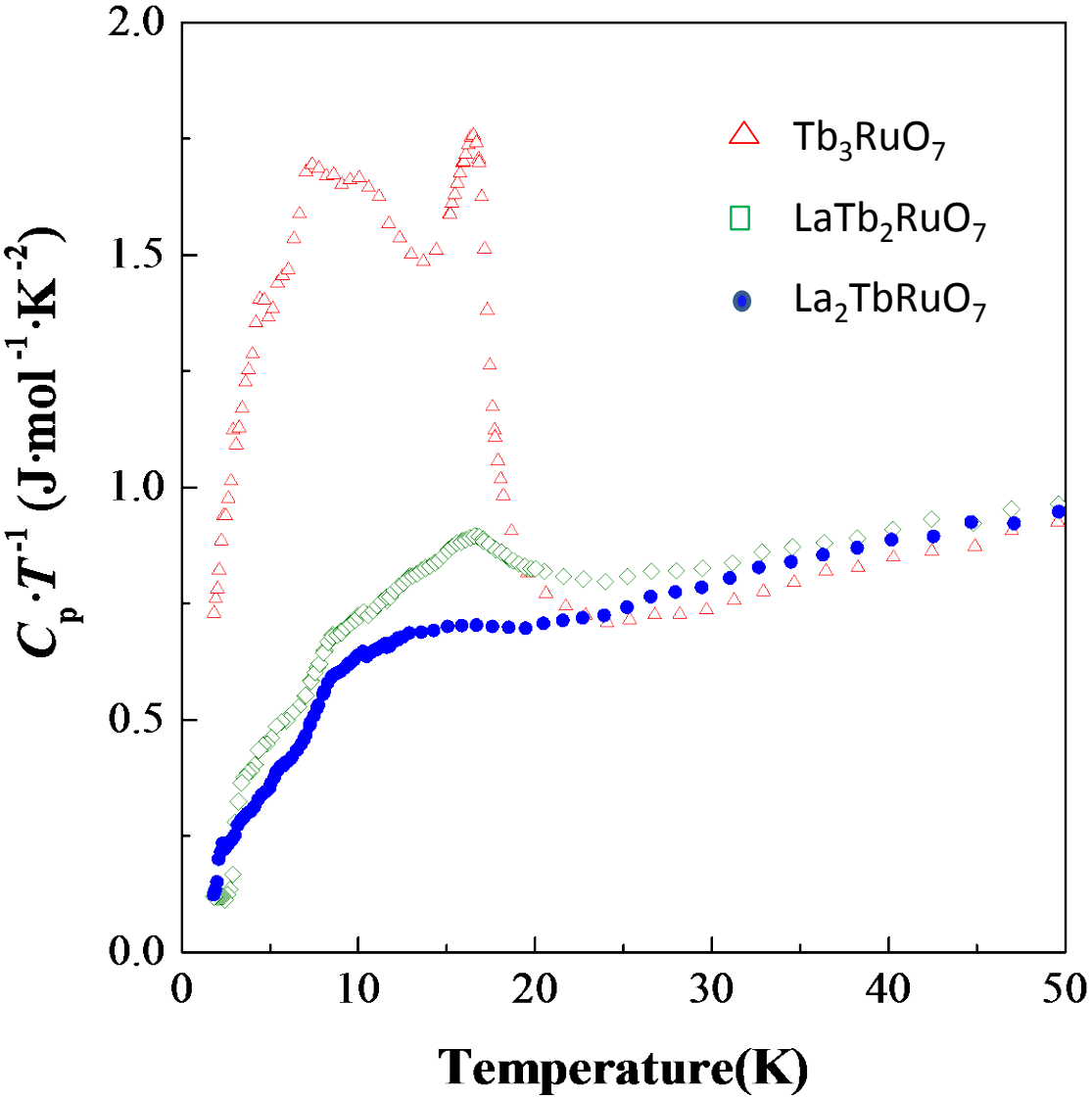
2.0
1.5
1.0
0.5
0.0
0
10
20
30
40
50
$C_p \cdot T^{-1}$ (J·mol^{-1}·K^{-2})
Temperature(K)
Tb_3RuO_7
$LaTb_2RuO_7$
La_2TbRuO_7

Fig. 8

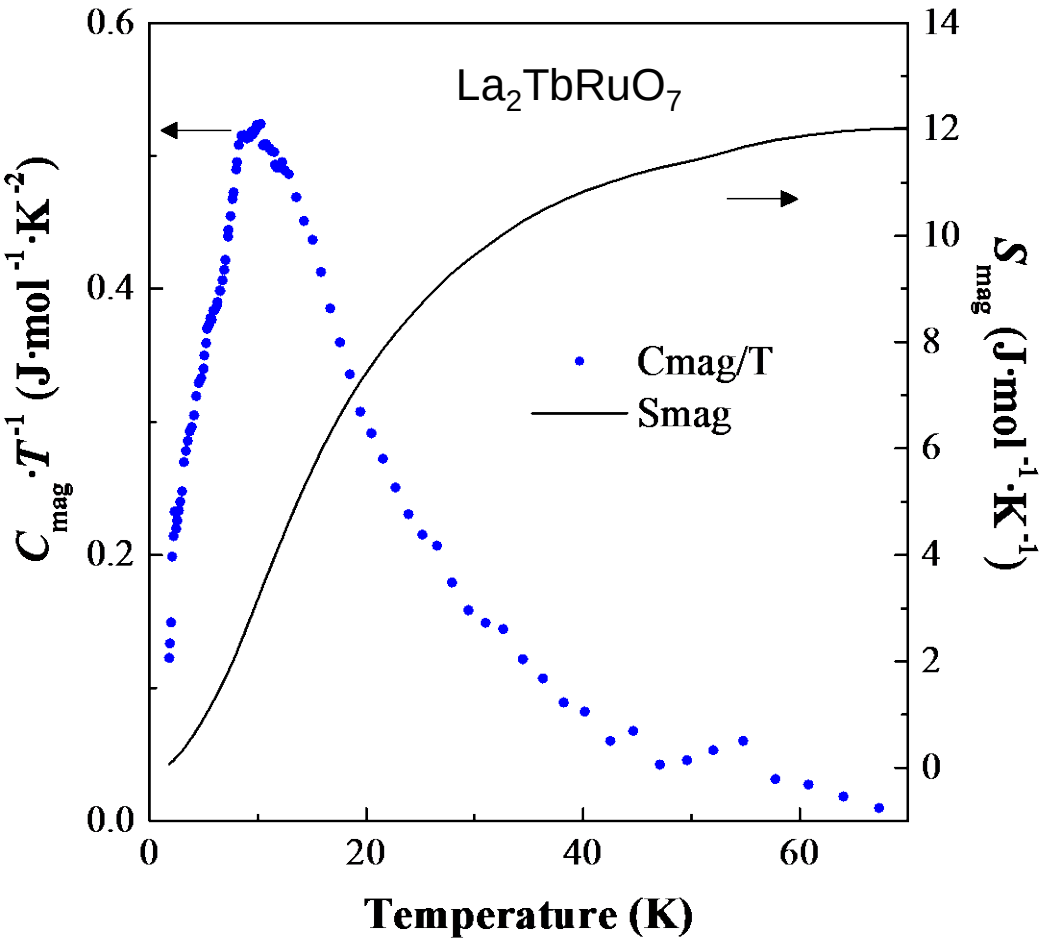
La2TbRuO7
Cmag/T
Smag
0.6
0.4
0.2
0.0
0
20
40
60
14
12
10
8
6
4
2
0
Temperature (K)
C_mag·T^-1 (J·mol^-1·K^-2)
S_mag (J·mol^-1·K^-1)

Fig.9